Journal of Solid State Chemistry 182 (2009) 1499–1505

Contents lists available at ScienceDirect

Journal of Solid State Chemistry

journal homepage: www.elsevier.com/locate/jssc

Solvothermal syntheses and structures of indium(III)-binaphthalenyl dicarboxylate complexes with yellow/blue luminescence

Qiang Gao [a,b], Fei-Long Jiang [a], Ming-Yan Wu [a], You-Gui Huang [a], Lian Chen [a], Wei Wei [a,b], Mao-Chun Hong [a,*]

[a] Key Laboratory of Optoelectronic Materials Chemistry and Physics, Fujian Institute of Research on the Structure of Matter, Chinese Academy of Sciences, Fuzhou 350002, PR China
[b] Graduate school of Chinese Academy of Science, Beijing, PR China

ARTICLE INFO

Article history:
Received 4 December 2008
Received in revised form
23 March 2009
Accepted 26 March 2009
Available online 5 April 2009

Keywords:
Indium(III)
Dihydroxy-binaphthyl-dicarboxylate
Crystal structure
Luminescence

ABSTRACT

Two novel In(III) complexes, $[In(bna)(Hbna)]_n$ (**1**) and $[In_2(bna)_2(\mu_2\text{-}OH)_2]_n \cdot 4nH_2O$ (**2**) (H_2bna = 2,2′-dihydroxy-1,1′-binaphthyl-3,3′-dicarboxylate acid), have been reported. Complex **1** adopts a 2D layer structure, where each layer composed from homochiral ligands is chiral while the ligands in two neighboring layers are enantiomer. Complex **2** is constructed by individual –In–O–In– chains, which are further connected by bna^{2-} into a 3D honeycomb framework. As a derivative of H_2bna ligand, dmbna (**3**) was recrystallized for structurally comparison with **1-2** (dmbna = dimethyl 2,2′-dihydroxy-1,1′-binaphthyl-3,3′-dicarboxylate). X-ray powder diffractions (XRD) and thermogravimetric analyses (TGA) for **1-2** show that they are highly thermally stable in the solid state. Complexes **1** and **2** exhibit the intense yellow luminescence at 573 nm and blue luminescence at 459 nm at room temperature, respectively. And an astonishing blue shift of 105 nm is observed for complex **1** when it is measured at 10 K.

1. Introduction

The design and synthesis of metal-organic frameworks (MOFs) have received much attention in recent years due to their potential applications in various research fields, such as gas adsorption and separation, catalysis, magnetism, and luminescence [1–13]. In order to obtain the MOFs with desirable topologies and properties, different metal ions and organic ligands were tested. For example, in order to construct complexes with remarkable photoluminescent properties, aromatic organic ligands and d^{10} metal ions deserve the researchers' intensive investigation. Aromatic organic ligands may display photoluminescence in the solid state [14–18], while the incorporation of d^{10} metal ions is found to be useful to enhance the luminescence intensity and lifetime of their hybrid complexes [19–21].

The optical active 2,2′-dihydroxy-1,1′-binaphthyl-3,3′-dicarboxylate acid (H_2bna) is a multifunctional ligand containing both carboxylic and phenolic groups, and can potentially afford various coordination modes and diverse MOF architectures. Meanwhile, the naphthyl rings can be severely twisted at different degrees across the C–C single bond due to steric effect, which may endow H_2bna with chirality. Free H_2bna displays weak luminescence in the solid state, and the photoluminescent property of its binaphthalene groups may be similar to those of other naphthalene derivatives, such as Hna (na = 3-hydroxy-naphthalene-2-carboxylate) [19–22]. The choice of metal ions is also important. The research results from our and some other groups indicate that In(III) is a good candidate for the construction of MOFs [23–40]. In contrast to the four- or six-coordinated fashions of divalent transition metal ions, In(III) ions have the ability to adopt MO_6 [23,25], MO_7 [23–25], or even MO_8 [26] coordination modes, which can benefit to the diversity of MOF framework, while the increased valence charge of In(III) may also show some influence on the resulting structures.

With above ideas in mind, we have selected indium(III) chloride and H_2bna to construct two novel hybrid complexes $[In(bna)(Hbna)]_n$ (**1**), $[In_2(bna)_2(\mu_2\text{-}OH)_2]_n \cdot 4nH_2O$ (**2**) by solvothermal method. As a derivative of H_2bna ligand, dmbna (**3**) was recrystallized from toluene during the synthesis of the ligand H_2bna for structurally comparison with **1** and **2** (dmbna = dimethyl 2,2′-dihydroxy-1,1′-binaphthyl-3,3′-dicarboxylate). Herein we report their syntheses, crystal structures and characterizations, including X-ray powder diffractions (XRD), thermogravimetric analyses (TGA) and photoluminescent studies. Their TGA show that **1** and **2** are highly thermally stable in the solid state. Complexes **1** and **2** exhibit the intense yellow luminescence at 573 nm and blue luminescence at 459 nm upon excitation at 365 nm at room temperature, respectively, and an astonishing blue shift of 105 nm is observed for **1** when it is measured at 10 K.

* Corresponding author. Fax: +86 591 83794946.
E-mail address: hmc@fjirsm.ac.cn (M.-C. Hong).

0022-4596/$ - see front matter © 2009 Elsevier Inc. All rights reserved.
doi:10.1016/j.jssc.2009.03.019

2. Experimental section

2.1. Materials and measurement

All chemicals were obtained from commercial sources and used without further purification. The racemic organic ligand H_2bna was synthesized according to the literature [41]. Elemental analyses were performed on a German Elementary Vario EL III instrument. The FT-IR spectra were recorded on a Nicolet Magna 750 FT-IR spectrometer using KBr pellets in the range of 4000–400 cm^{-1}. Thermogravimetric analyses were carried out on a NETZSCH STA 449 C unit at a heating rate of 10 °C/min under nitrogen atmosphere. Photoluminescence analyses were performed on a Perkin-Elemer LS55 fluorescence spectrometer. The power X-ray diffraction patterns of the as-synthesized samples were recorded by a RIGAKU-DMAX2500 X-ray diffractometer using Cu$K\alpha$ radiation ($\lambda = 0.154$ nm) at a scanning rate of 5°/min for 2θ ranging from 5° to 85°. N_2 adsorption isotherms in the pressure range of 0–1.0 bar were measured using a Micromeritics ASAP2020 instrument at 77 K.

2.2. Syntheses of $[In(bna)(Hbna)]_n$ (**1**), $[In_2(bna)_2(\mu_2\text{-}OH)]_n \cdot 4nH_2O$ (**2**) and dmbna (**3**)

A mixture of $InCl_3 \cdot 4H_2O$ (58.0 mg, 0.2 mmol), H_2bna (76.0 mg, 0.2 mmol), 4,4′-trimethylenedipiperidine (47.0 mg, 0.2 mmol), water (5 ml) and methanol (5 ml) with the pH value around 5 was placed in 30 ml Teflon-lined stainless steel autoclave. The autoclave was sealed, heated to 140 °C under autogenous pressure for 96 h, and then cooled to room temperature at 6 °C h^{-1}. Block colorless crystal of complex **1** was obtained with some impurity, manual separation gives about 100 mg of complex **1** (yield 60% based on H_2bna). The phase purity of the bulk products was checked by comparing its observed and simulated XRD patterns. Elemental analysis for $C_{44}H_{25}InO_{12}$ (Mr = 860.46): calcd: C 61.42%, H 2.93%; found: C 61.81%, H 2.08%. Selected IR data (KBr pellet, cm^{-1}): 3467 (br, w), 3173 (s), 2952 (m), 1682 (s), 1625 (w), 1503 (s), 1442 (s), 1326 (m), 1285 (m), 1224 (s), 1152 (m), 1083 (m), 933 (m), 797 (s), 708 (m).

A mixture of $InCl_3 \cdot 4H_2O$ (58.0 mg, 0.2 mmol), H_2bna (76.0 mg, 0.2 mmol), imidazole (34.0 mg, 0.5 mmol), water (5 ml) and ethanol (5 ml) with the pH value around 4 was placed in 30 ml Teflon-lined stainless steel autoclave. The autoclave was sealed, heated to 120 °C under autogenous pressure for 96 h, and then cooled to room temperature at 6 °C h^{-1}. Light yellow crystalline product was filtered, washed with distilled water, and dried at ambient temperature to give about 150 mg of complex **2** (yield 70% based on H_2bna). The phase purity of the bulk products was checked by comparing its observed and simulated XRD patterns. Elemental analysis for $C_{44}H_{34}In_2O_{18}$ (Mr = 1080.35): calcd: C 48.92%, H 3.17%; found: C 49.11%, H 3.14%. Selected IR data (KBr pellet, cm^{-1}): 3504 (w), 3216 (s), 1636 (s), 1585 (w), 1547 (s), 1502 (w), 1460 (s), 1422 (m), 1399 (s), 1334 (m), 1288 (m), 1239 (w), 1151 (w), 806 (w), 935 (w), 806 (s), 747 (s), 603 (w).

Compound **3** was obtained by recrystallization from toluene during the synthesis of the ligand H_2bna. Elemental analysis for $C_{24}H_{18}O_6$ (Mr = 402.38): calcd: C 71.64%, H 4.51%; found: C 71.68%, H 4.54%. Selected IR data (KBr pellet, cm^{-1}): 3171 (br, s), 2949 (m), 1682 (s), 1623 (m), 1503 (s), 1442 (s), 1326 (s), 1285 (m), 1224(s), 1152 (m), 1083 (s), 933 (w), 797 (s), 705 (m).

2.3. Single-crystal structure determination

Single crystals of compounds **1**–**3** were mounted on either a Rigaku Mercury CCD diffractometer (for **1**) or a RIGAKU SATURN70 (for **2** and **3**), both equipped with a graphite-monochromated Mo$K\alpha$ radiation ($\lambda = 0.71073$ Å). Intensity data were collected by the narrow frame method at 293 K. All three structures were solved by the direct methods and refined by full-matrix least-squares fitting on F^2 by SHELX-97 [42]. All non-hydrogen atoms except free water molecules O16, O17, O18 atoms in **2** were refined with anisotropic thermal parameters. Hydrogen atoms excluding those for water molecules and those associated with μ_2-O in complex **2** were located at geometrically calculated positions and refined with isotropical thermal parameters. Crystallographic data and structural refinements for compounds **1**–**3** are summarized in Table 1. Selected bond lengths and bond angles are listed in Tables 2 and 3. More details on the crystallographic studies as well as atomic displacement parameters are given as Supporting information as CIF files.

Table 1
Crystallographic data for **1**–**3**.

Identification code	**1**	**2**	**3**
Empirical formula	$C_{44}H_{25}InO_{12}$	$C_{44}H_{34}In_2O_{18}$	$C_{24}H_{18}O_6$
Formula weight	860.46	1080.35	402.38
Crystal system	Orthorhombic	Trigonal	Monoclinic
Space group	*Ccca*	*R*-3	$P2_1/n$
a (Å)	12.854 (5)	34.716 (5)	10.352 (4)
b (Å)	18.706 (7)	34.716 (5)	9.068 (3)
c (Å)	22.287 (8)	20.114 (4)	21.211 (7)
α (deg)	90	90	90
β (deg)	90	90	98.048 (6)
γ (deg)	90	120	90
V (Å^3)	5359 (3)	20994 (5)	1971.5 (12)
Z	4	18	4
Dc (g/cm^{-3})	1.067	1.538	1.356
μ (mm^{-1})	0.488	1.061	0.098
Goodness-of-fit on F^2	1.175	1.107	1.091
Final *R* indices	$R_1 = 0.0797$,	$R_1 = 0.0473$,	$R_1 = 0.0643$,
$[I > 2\sigma(I)]$[a]	$wR_2 = 0.2110$	$wR_2 = 0.1143$	$wR_2 = 0.1797$
R indices (all data)	$R_1 = 0.1029$,	$R_1 = 0.0537$,	$R_1 = 0.1147$,
	$wR_2 = 0.2277$	$wR_2 = 0.1188$	$wR_2 = 0.2185$

[a] $R1 = \Sigma||F_o|-|F_c||/\Sigma|F_o|$. $wR_2 = [\sum w(F_0^2 - F_c^2)^2 / \sum w(F_0^2)^2]^{1/2}$.

3. Results and discussion

3.1. Syntheses

Several methods have been applied in the design and construction of new inorganic–organic hybrid compounds with multifunctional ligands. Among these methods, hydrothermal or solvothermal synthesis has been proved to be an efficient one. Complexes **1** and **2** reported here were synthesized by solvothermal method, in which the choice of solvents and deprotonation reagents is important. During the syntheses of **1**–**2**, methanol and ethanol were used, respectively. As is known, several properties of the above two solvents are different, such as solution capability, boiling point, and polarity, which may be the most remarkable factors that influence the resulting structures of hybrid complexes. Furthermore, different organic bases (4,4′-trimethylenedipiperidine and imidazole) are used during the reactions. Comparing 4,4′-trimethylenedipiperidine with imidazole, the pKb value of the former is much lower than the latter, and the pH value of the reaction system for **1** is higher than that for **2**. However, replacing these two organic bases with other bases to adjust the reaction solutions to the previous pH values failed to reproduce complexes **1** and **2**. So the organic bases we used here may not just act as deprotonation reagents, but also play an important role in directing the construction of the final products.

Table 2
Selected bond lengths (Å) and bond angles (deg) for **1**–**3**.

1			
In1—O3	2.215 (4)	In1—O2	2.350 (5)
$O3^{i}$—In1—O3	133.3 (2)	$O2^{iii}$—In1—O2	172.65 (18)
$O3^{i}$—In1—$O3^{ii}$	74.4 (2)	O2—In1—$O2^{i}$	88.0 (2)
O3—In1—$O3^{ii}$	125.7 (2)	O3—In1—$O2^{i}$	88.79 (16)
O3—In1—$O2^{iii}$	130.68 (15)	O3—In1—$O2^{ii}$	85.35 (16)
O3—In1—O2	56.66 (14)	O2—In1—$O2^{ii}$	92.5 (2)
Symmetry codes: (i) x, 1/2−y, 1/2−z; (ii) −x, 1/2−y, z; (iii) −x, y, 1/2−z			
2			
In1—O14	2.070 (3)	In2—$O14^{iii}$	2.061 (3)
In1—O13	2.077 (3)	In2—O13	2.069 (3)
In1—$O1^{i}$	2.157 (3)	In2—$O2^{iv}$	2.156 (3)
In1—O8	2.177 (3)	In2—O7	2.159 (3)
In1—O5	2.181 (3)	In2—O4	2.177 (3)
In1—$O12^{ii}$	2.203 (3)	In2—$O11^{v}$	2.196 (3)
O14—In1—O13	94.99 (11)	$O14^{iii}$—In2—O13	175.08 (11)
O14—In1—$O1^{i}$	88.78 (11)	$O14^{iii}$—In2—$O2^{iv}$	94.69 (11)
O13—In1—$O1^{i}$	175.55 (11)	O13—In2—$O2^{iv}$	90.17 (11)
O14—In1—O8	164.12 (11)	$O14^{iii}$—In2—O7	87.90 (11)
O13—In1—O8	97.14 (11)	O13—In2—O7	91.52 (12)
$O1^{i}$—In1—O8	79.59 (11)	$O2^{iv}$—In2—O7	87.74 (13)
O14—In1—O5	102.45 (11)	$O14^{iii}$—In2—O4	89.91 (11)
O13—In1—O5	95.24 (11)	O13—In2—O4	85.34 (11)
$O1^{i}$—In1—O5	81.61 (11)	$O2^{iv}$—In2—O4	172.54 (12)
O8—In1—O5	86.62 (11)	O7—In2—O4	98.30 (13)
O14—In1—$O12^{ii}$	91.03 (11)	$O14^{iii}$—In2—$O11^{v}$	90.85 (11)
O13—In1—$O12^{ii}$	89.86 (11)	O13—In2—$O11^{v}$	89.67 (11)
$O1^{i}$—In1—$O12^{ii}$	92.44 (11)	$O2^{iv}$—In2—$O11^{v}$	92.97 (12)
O8—In1—$O12^{ii}$	78.81 (10)	O7—In2—$O11^{v}$	178.61 (13)
O5—In1—$O12^{ii}$	165.07 (11)	O4—In2—$O11^{v}$	81.08 (11)
Symmetry codes: (i) x, 1+y, z; (ii) x, y, −1+z; (iii) 2/3−x+y, 4/3−x, 1/3+z (iv) x, −1+y, z; (v) x, y, 1+z			
3			
O1—C11	1.206 (3)	O4—C24	1.364 (3)
O2—C11	1.331 (3)	O5—C22	1.220 (3)
O2—C12	1.467 (4)	O6—C22	1.335 (3)
O3—C10	1.356 (3)	O6—C23	1.445 (4)
C11—O2—C12	115.6 (3)	C22—O6—C23	115.6 (3)

Table 3
Photoluminescent lifetime data for complexes **1** and **2**

Complex	Lifetime (ns)	
	τ_1	τ_2
1 (RT)	0.850 (95.55%)	5.719 (4.45%)
1 (10 K)	2.235 (33.23%)	5.967 (66.77%)
2	1.561 (69.14%)	0.326 (30.86%)

3.2. Structure description for compounds ***1–3***

3.2.1. Complex $[In(bna)(Hbna)]_n$ (***1***)

Complex **1** crystallizes in an orthorhombic space group *Ccca*. As shown in Fig. 1, In(III) ion is eight-coordinated by eight oxygen atoms from four carboxylic groups of four independent bna^{2-} ligands. It forms a decahedron motif, which exhibits high coordinating ability of In(III) ions, with the In–O bond lengths of 2.215 (4) and 2.350 (5) Å (see Table 2). The dihedral angle between the pair of naphthyl rings of the ligand is 80.6°. The coordination modes of bna^{2-} in this article are schematically represented in Scheme S1. The carboxylic groups of bna^{2-} ligand can chelate one metal ion in a bidentate mode, or coordinate to two metal centers in an O, O′ mode, while its phenolic groups are not engaged in the coordination. In complex **1**, the bna^{2-} ligand adopts coordination mode **A**. In order to balance the charge, one of the two ligands is monoprotonated, but it is hard to locate the hydrogen atom crystallographically. The ligands connect the metal centers to form a chain along [010] direction. The twisted conformation of the ligand endows the chain with chirality. Furthermore, these helices are interconnected through the metal centers, resulting in a 2D wavelike chiral layer structure (Fig. 2). In this plane, all the ligands are homochiral. If we treat the metal centers as the nodes and the ligands as the linear linkers, then the layer can be viewed as a (4, 4) grid structure. This layer interdigitates with one of two neighboring layers and forms a two-fold packing unit. It is interesting that the ligands from the two neighboring layers are enantiomer, leading to the opposite chirality of these two neighboring planes. These layers with opposite chirality pack alternatively along *c* axis (Fig. 3). Thus, the structure of complex **1** is achiral.

3.2.2. Complex $[In_2(bna)_2(\mu_2\text{-}OH)]_n \cdot 4nH_2O$ (***2***)

There are two In(III) ions, two bna^{2-} ligands, two groups of μ_2-OH and four guest water molecules in the asymmetric unit of complex **2**. As illustrated in Fig. 4, each In(III) center is coordinated by four oxygen atoms from four independent bna^{2-} ligands and by two oxygen atoms from two μ_2-OH groups, where the latter two occupy the apical positions to fulfill the octahedron coordination motif. The μ_2-OH groups may come from the water molecules, as the reaction was performed under the solvothermal condition, which is not infrequent according to the literature even in the

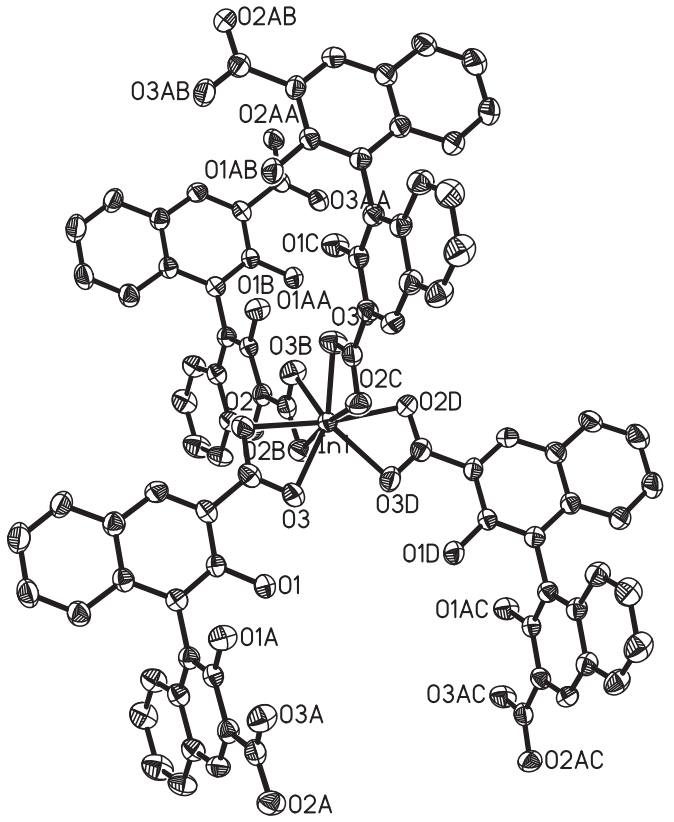

Fig. 1. The coordination environment around In(III) in **1** with the thermal ellipsoid at the 30% probability level. Symmetry code: A: $-1/2-x, -y, z$; B: $x, 1/2-y, 1/2-z$; C: $-x, 1/2-y, z$; D: $-x, y, 1/2-z$.

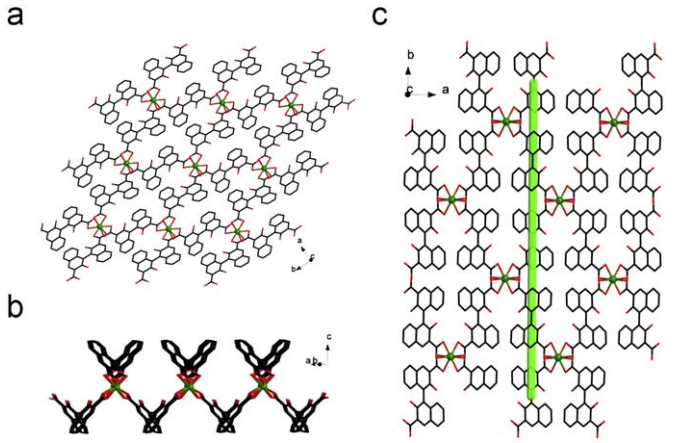

Fig. 2. (a) Schematic representation of the 2D chiral layer, (b) side view of the layer, and (c) VIEW of the 2_1 helix of the layer along *b* axis.

acidic environment [34]. The In-O bond lengths range from 2.061 (3) to 2.203 (3) Å (see Table 2). All the bna^{2-} ligands in complex **2** adopt coordination mode **B** and the dihedral angle between the pair of naphthyl rings of the ligand is 81.7° for $bna^{2-}(1)$ and 75.3° for $bna^{2-}(2)$, respectively. The two μ_2-OH joint In(III) centers into a infinite –In–O–In– chain along the *c* axis (Fig. 5a). Furthermore, one $bna^{2-}(1)$ ligand and one $bna^{2-}(2)$ ligand both act as the linkers to bind two such chains together. From another point of view, each chain is interconnected to three adjacent chains by three $bna^{2-}(1)$ ligands and three $bna^{2-}(2)$ ligands. In this way, the ligands joint the chains into a double-wall honeycomb framework (Fig. 5b). There are two types of channels running along the [001]

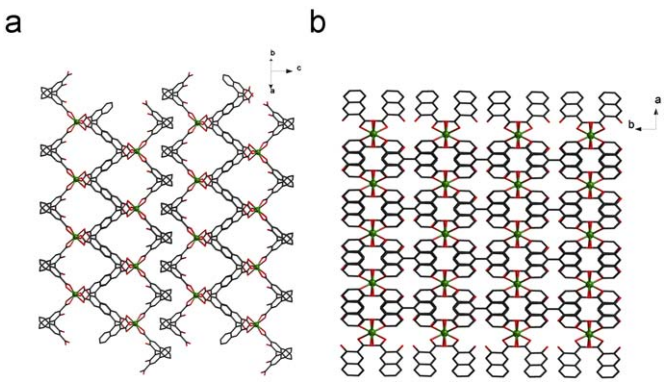

Fig. 3. (a) Interdigitation and packing mode of **1** along [110] direction and (b) view of packing of **1** along [100] direction.

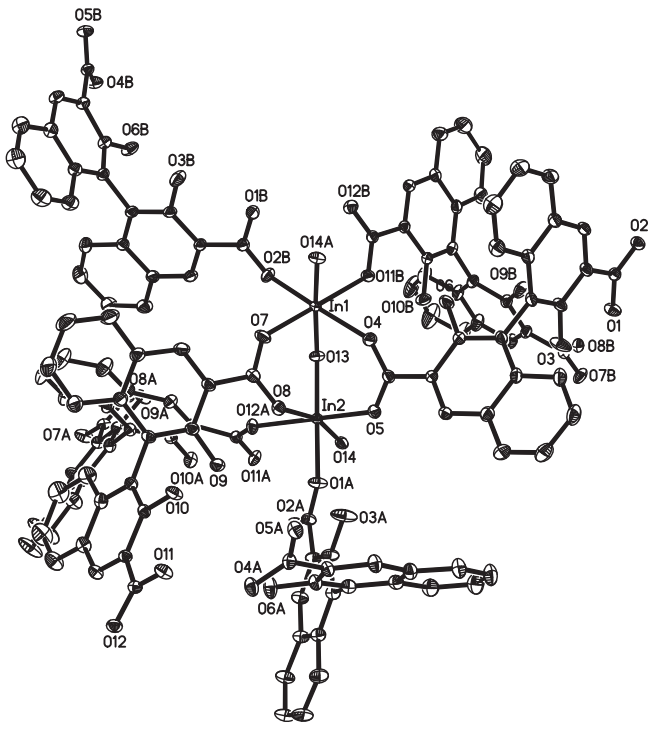

Fig. 4. The coordination environment around In(III) in **2** with the thermal ellipsoid at the 30% probability level. Symmetry code: A: $x, 1+y, z$; B: $x, y, -1+z$; C: $2/3-x+y, 4/3-x, 1/3+z$; D: $x, -1+y, z$; E: $x, y, 1+z$.

direction, one is formed by the double-wall motif and the other surrounded by naphthyl rings. The phenolic groups protrude into the first type of channels and make the channels hydrophilic; the guest water molecules are all located in these channels and form various hydrogen bonds with the phenolic groups. On the contrary, the other channels are hydrophobic and no guest water molecules are found in them (Fig. 5c).

The total solvent-accessible volume in the unit cell is 2397.0 $Å^3$ for **1** and 5000.9 $Å^3$ for **2**, which accounts for 44.7% and 23.8% of the total cell volume as calculated by PLATON, respectively [43]. Investigations of N_2 adsorption property was performed on **1** and **2**, the results indicated that there were no obvious adsorptions for N_2.

3.2.3. *Compound dmbna (**3**)*

The structure of compound **3** features a 3D supramolecular network. As shown in Fig. S1, the asymmetric unit contains one

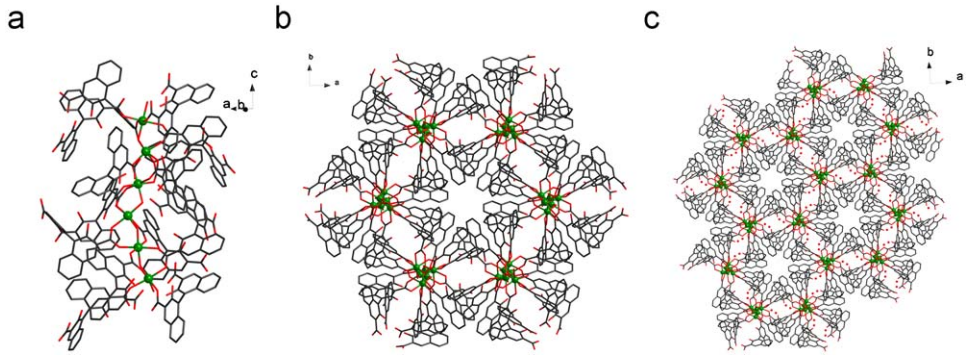

Fig. 5. (a) View of 1D –In–O–In– chain along [001] direction; (b) schematic representation of the double-wall honeycomb structure; (c) view of packing of **2** along [001] direction, the two types of channels are clearly shown, with one filled with guest water molecules.

dmbna molecule. Compound **3**, as a derivative of H_2bna ligand for structurally comparison with **1** and **2**, its dihedral angle between the pair of naphthyl rings is 80.0°. The two phenolic groups of dmbna compound form two groups of intramolecular hydrogen bonds with the oxygen atoms from the ortho-carboxylic groups (see Table S1). The dmbna molecule interacts with three other adjacent molecules through π–π stacking interactions and non-classical hydrogen bonding interactions (CH$\cdots\pi$ interactions) (Fig. S2). The centroid-to-centroid distance is 3.894 Å, the C–H$\cdots$phenyl centroid distance is 2.780 Å and the C–H$\cdots$phenyl centroid angle is 157.76°. It is worth noting that the two molecules interacting through π–π stacking interactions are enantiomer, while other two molecules through CH$\cdots\pi$ interactions are homochiral. The asymmetric units are assembled into a 2D plane through these two kinds of interactions, then the planes further pack along *c* axis (Fig. S2).

We try to find the relationship between the coordination modes and the dihedral angles between the pair of naphthyl rings of bna^{2-} ligands. As illustrated in Scheme S2, six types of coordination modes of bna^{2-} are found in the literature. The corresponding angles are listed in Table S2. However, even in coordination mode **B**, the dihedral angles between the pair of naphthyl rings of bna^{2-} vary in a large range from 74.1° to 94.6°. In coordination mode **A**, the dihedral angles also change from 67.0° to 80.6°. It seems that their dihedral angles are influenced not only by coordination modes; but also by connectivity and the frameworks.

3.3. Thermogravimetric analyses, X-ray powder diffraction and IR spectra

The thermogravimetric analyses were performed on complexes **1** and **2** to investigate the thermal stability. As shown in Fig. S3, the TGA curve of complex **1** indicates its high thermal stability up to 320 °C, and then the framework collapses in two steps. Complex **2** gradually loses it lattice water from 40 to 345 °C (found. 6.4%, calcd. 6.7%), then it decomposes rapidly.

In order to check the phase purity of these complexes, the X-ray powder diffraction of complexes **1** and **2** were measured at room temperature. The peak positions of simulated XRD patterns match with those observed ones, indicating that the complexes are obtained in pure phases (Fig. S4). The differences in intensity may be due to the preferred orientation of the crystalline powder samples.

The FT-IR spectra of compounds **1** to **3** are represented in Fig. S5 (see supporting information). The range of 1637–1505 cm^{-1} for **1**, 1636–1547 cm^{-1} for **2** and 1683–1623 cm^{-1} for **3** are the characteristic bands of carboxylate groups for asymmetric stretching, while the range of 1460–1396 cm^{-1} (**1**), 1460–1399 cm^{-1} (**2**) and 1442–1326 cm^{-1} (**3**) for symmetric stretching. Furthermore, the weak absorption peaks at 3179 cm^{-1} for **1**, 3217 cm^{-1} for **2** and 3171 cm^{-1} for **3** can be attributed to the hydroxyl groups from the ligands.

3.4. Photoluminescent properties

The photoluminescence spectra of complexes **1** and **2** were recorded in the solid state at room temperature and at 10 K. As illustrated in Fig. 6, complex **1** exhibits an intense yellow luminescence at 573 nm ($\lambda_{ex}=365$ nm) at room temperature. However, at 10 K, the emission spectrum of **1** shows the sharp peak at 468 nm ($\lambda_{ex}=420$ nm), which is an astonishing blue shift of 105 nm compared with that at room temperature. Complex **2** exhibits intense pure blue photoluminescence with an emission maximum at ca. 459 nm upon excitation at 365 nm, and the blue emission could even be observed by naked eyes under irradiation of ultraviolet light with the wavelength of 365 nm. Usually, two types of transition, namely, ligand-to-ligand charge transfer (LLCT) and ligand-to-metal charge transfer (LMCT), would be proposed for the photoluminescence emissions of such In(III) coordination complexes. However, it is difficult to determine the correct mechanism for the luminescence barely based on the emission spectra, thus the excited-state lifetime (τ) measurements may be helpful. For complexes **1** and **2**, the decay is best described by a biexponential process (see Table 3). The corresponding lifetimes for complex **1** are $\tau_1=0.850$ ns and $\tau_2=5.719$ ns at room temperature, $\tau_1=2.235$ ns and $\tau_2=5.967$ ns at 10 K, while the life time for **2** are $\tau_1=1.561$ ns and $\tau_2=0.326$ ns at room temperature. According to the analyses of bna^{2-} containing coordination polymers, the emission bands for complexes **1** and **2** may be assigned to LLCT, admixing with LMCT transitions [19].

4. Conclusion

In summary, two novel In(III)-bna^{2-} complexes **1**–**2** have been synthesized under hydrothermal condition. In(III) ions from compplexes **1** and **2** are eight and six-coordinated, respectively, demonstrating the diversity of coordination motif for In(III) ions. The bna^{2-} ligands adopt (κ^2-κ^2)-μ_2 in 1 and (κ^1-κ^1)-(κ^1-κ^1)-μ_4 coordination mode in **2**. Complex **1** has a 2D layer structure, and the bna^{2-} ligands in two neighboring layers are enantiomer. In **2**, the bna^{2-} ligands joint the infinite –In–O–In– chains into a double-wall honeycomb framework. Our results reveal that the choice of organic base is important in constructing the MOFs.

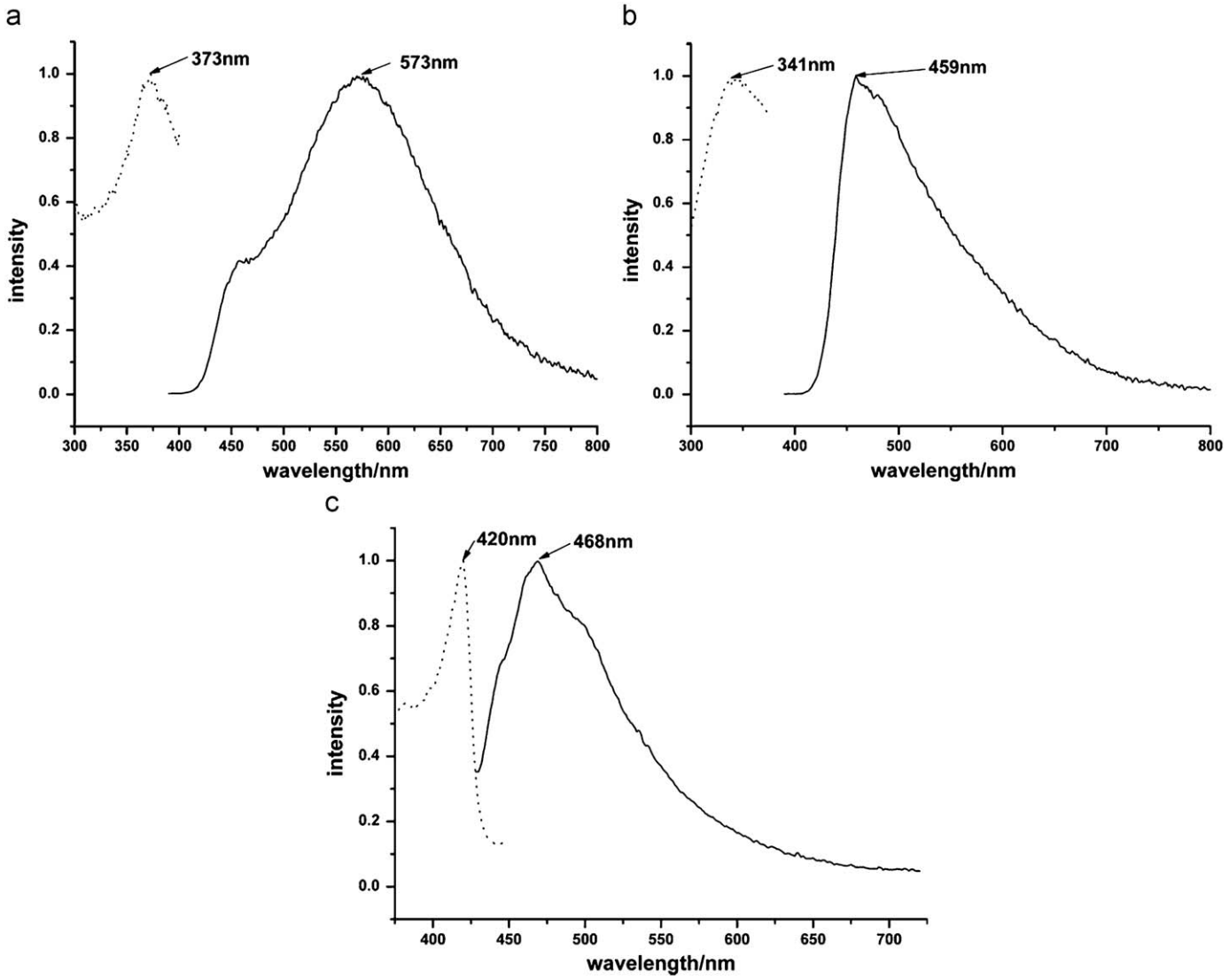

Fig. 6. Solid-state photoluminescence spectra of complexes **1** (a), **2** (b) at room temperature and at 10 K for **1**(c).

Furthermore, the intense yellow/blue luminescences of complexes **1** and **2** may have potential applications in photoactive materials.

Acknowledgment

This work was supported by grants from the National Natural Science Foundation of China and the Natural Science Foundation of Fujian Province.

Appendix A. Supplementary material

Supplementary data associated with this article can be found in the online version at doi:10.1016/j.jssc.2009.03.019.

References

[1] M. Eddaoudi, J. Kim, N. Rosi, D. vodka, J. Wachter, M. O'Keeffe, O.M. Yaghi, Science 295 (2002) 469–472.
[2] R. Matsuda, R. Kitaura, S. Kitagawa, Y. Kubota, R.V. Belosludov, T.C. Kobayashi, H. Salamoto, T. Chiba, M. Takata, Y. Kawazoe, Y. Mita, Nature 436 (2005) 238–241.
[3] C.D. Wu, W.B. Lin, Angew. Chem. Int. Ed. 44 (2005) 1958–1961.
[4] D.F. Sun, S.Q. Ma, Y.X. Ke, D.J. Collins, H.C. Zhou, J. Am. Chem. Soc. 128 (2006) 3896–3897.
[5] B. Gomez-Lor, E. Gutiérrez-Puebla, M. Lglesias, M.A. Monge, C. Ruiz-Valero, N. Snejko, Inorg. Chem. 41 (2002) 2429–2432.
[6] M. Yoshizawa, M. Tamura, M. Fujita, Science 312 (2006) 251–254.
[7] S.C. Xiang, X.T. Wu, J.J. Zhang, R.B. Fu, S.M. Hu, X.D. Zhang, J. Am. Chem. Soc. 127 (2005) 16352–16353.
[8] A.B. Gaspar, V. Ksenofontov, V. Martinez, M.C. Muñoz, J.A. Real, P. Gütlich, Eur. J. Inorg. Chem. (2004) 4770–4773.
[9] J. Pang, E.J.P. Marcotte, C. Seward, R.S. Brown, S.N. Wang, Angew. Chem. Int. Ed. 40 (2001) 4042–4045.
[10] L.H. Gao, M. Guan, K.Z. Wang, L.P. Jin, C.H. Huang, Eur. J. Inorg. Chem. (2006) 3731.
[11] R.K. Feller, A.K. Cheetham, Dalton Trans. (2008) 2034–2042.
[12] H.W. Wang, S. Gao, L.H. Huo, S.W. Ng, J.G. Zhao, Cryst. Growth Des. 8 (2008) 665–670.
[13] J.L. Du, T.L. Hu, J.R. Li, S.M. Zhang, X.H. Bu, Eur. J. Inorg. Chem. (2008) 1059–1066.
[14] D. Tanaka, S. Horike, S. Kitagawa, M. Ohba, M. Hasegawa, Y. Ozawac, K. Toriumic, Chem. Commun. (2007) 3142–3144.
[15] J.J. Wang, C.S. Liu, T.L. Hu, Z. Chang, C.Y. Li, L.F. Yan, P.Q. Chen, X.H. Bu, Q. Wu, L.J. Zhao, Z. Wang, X.Z. Zhang, Cryst. Eng. Commun. (2008) 681–692.
[16] J.M. Herrera, S.J.A. Pope, A.J.H.M. Meijer, T.L. Easun, H. Adams, W.Z. Alsindi, X.Z. Sun, M.W. George, S. Faulkner, M.D. Ward, J. Am. Chem. Soc. 129 (2007) 11491–11504.
[17] G.J. McManus, J.J. Perry IV, M. Perry, B.D. Wagner, M.J. Zaworotko, J. Am. Chem. Soc. 129 (2007) 9094–9101.
[18] C.A. Bauer, T.V. Timofeeva, T.B. Settersten, B.D. Patterson, V.H. Liu, B.A. Simmons, M.D. Allendorf, Am. Chem. Soc. 129 (2007) 7136–7144.

[19] L.Y. Zhang, J.P. Zhang, Y.Y. Lin, X.M. Chen, Cryst. Growth Des. 6 (2006) 1684–1689.
[20] S.L. Zheng, M.L. Tong, S.D. Tan, Y. Wang, J.X. Shi, Y.X. Tong, H.K. Lee, X.M. Chen, Organometallics 20 (2001) 5319–5325.
[21] S.L. Zheng, J.H. Yang, X.L. Yu, X.M. Chen, W.T. Wong, Inorg. Chem. 43 (2004) 430–438.
[22] L.P. Lu, S.D. Qin, P. Yang, M.L. Zhu, Acta Crystallogr. Section E 60 (2004) m950–m952.
[23] Z.Z. Lin, F.L. Jiang, L. Chen, D.Q. Yuan, Y.F. Zhou, M.C. Hong, Eur. J. Inorg. Chem. (2005) 77–81.
[24] Z.Z. Lin, F.L. Jiang, L. Chen, D.Q. Yuan, M.C. Hong, Inorg. Chem. 44 (2005) 73–76.
[25] Z.Z. Lin, F.L. Jiang, D.Q. Yuan, L. Chen, Y.F. Zhou, M.C. Hong, Eur. J. Inorg. Chem. (2005) 1927–1931.
[26] Z.Z. Lin, F.L. Jiang, L. Chen, C.Y. Yue, D.Q. Yuan, A.J. Lan, M.C. Hong, Cryst. Growth Des. 7 (2007) 1712–1715.
[27] Z.Z. Lin, J.H. Luo, M.C. Hong, R.H. Wang, L. Han, R. Cao, J. Solid State Chem. 177 (2004) 2494–2498.
[28] Z.Z. Lin, L. Chen, F.L. Jiang, M.C. Hong, Inorg. Chem. Commun. 8 (2005) 199–201.
[29] Y.I. Liu, J.F. Eubank, A.J. Cairns, J. Eckert, V.Ch. Kravtsov, R. Luebke, M. Eddaoudi, Angew. Chem. Int. Ed. 46 (2007) 3278–3283.
[30] J.L. Belof, A.C. Stern, M. Eddaoudi, B. Space, J. Am. Chem. Soc. 129 (2007) 15202–15210.
[31] B. Gómez-Lor, E. Gutiérrez-Puebla, M. Iglesias, M.A. Monge, C. Ruiz-Valero, N. Snejko, Inorg. Chem. 41 (2002) 2429–2432.
[32] B. Gómez-Lor, E. Gutiérrez-Puebla, M. Iglesias, M.A. Monge, C. Ruiz-Valero, N. Snejko, Chem. Mater. 14 (2005) 2568–2573.
[33] M. Vougo-Zanda, X.Q. Wang, A.J. Jacobson, Inorg. Chem. 46 (2007) 8819–8824.
[34] Z.G. Guo, Y.F. Li, W.B. Yuan, X.D. Zhu, X.F. Li, R. Cao, Eur. J. Inorg. Chem. (2008) 1326–1331.
[35] X.M. Liu, G.H. Li, B. Hu, Y. Yu, Y.W. Hu, M.H. Bi, Z. Shi, S.H. Feng, Eur. J. Inorg. Chem. (2008) 2522–2529.
[36] J. Su, Y.X. Wang, S.H. Yang, G.B. Li, F.H. Liao, J.H. Lin, Inorg. Chem. 46 (2007) 8403–8409.
[37] E.V. Anokhina, M. Vougo-Zanda, X.Q. Wang, A.J. Jacobson, J. Am. Chem. Soc. 127 (2005) 15000–15001.
[38] S. Das, C.H. Hung, S. Goswami, Inorg. Chem. 42 (2003) 5153–5157.
[39] Y.L. Liu, V.Ch. Kravtsov, D.A. Beauchamp, J.F. Eubank, M. Eddaoudi, J. Am. Chem. Soc. 127 (2005) 7266–7267.
[40] C. Chen, Y.L. Liu, S.H. Wang, G.H. Li, M.H. Bi, Z. Yi, W.Q. Pang, Chem. Mater. 18 (2006) 2950–2958.
[41] M. Nakajima, I. Miyoshi, K. Kanayama, S.I. Hashimoto, J. Org. Chem. 64 (1999) 2264–2271.
[42] G.M. Sheldrick, SHELXTL-97, Program for the Solution of Crystal Structures; University of Göttingen: Germany 1997.
[43] A.L. Spek, PLATON-A Multipurpose Crystallographic Tool, Utrecht University, Netherlands, 2000.